Molecular Mobility of a Polymer of Intrinsic Microporosity Revealed by Quasielastic Neutron Scattering

Reiner Zorn[1], Wiebke Lohstroh[2], Michaela Zamponi[3], Wayne J. Harrison[4], Peter M. Budd[4], Martin Böhning[5], Andreas Schönhals[5,]*

[1]Forschungszentrum Jülich GmbH, Jülich Centre for Neutron Science (JCNS-1), 52425 Jülich, Germany

[2]Heinz Maier-Leibnitz Zentrum (MLZ), Technische Universität München, Lichtenbergstraße 1, 85748 Garching, Germany

[3]Forschungszentrum Jülich GmbH, Jülich Centre for Neutron Science at MLZ, Lichtenbergstr. 1, 85748 Garching, Germany

[4]The University of Manchester, Department of Chemistry, Manchester M13 9PL, United Kingdom

[5]BAM Bundesanstalt für Materialforschung und -prüfung, Unter den Eichen 87, 12205 Berlin, German

RECEIVED DATE:

[*]CORRESPONDING AUTHOR: A. Schönhals, BAM Bundesanstalt für Materialforschung und -prüfung (Fachbereich 6.6), Unter den Eichen 87, 12205 Berlin, Germany; Tel. +49 30 / 8104-3384; Fax: +49 30 / 8104-1637; Email: Andreas.Schoenhals@bam.de

For TOC graphic entry only

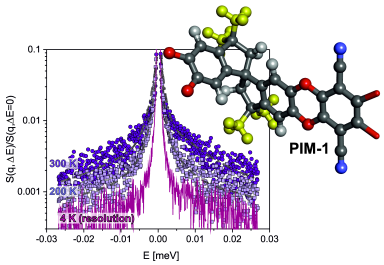

ABSTRACT:

Quasielastic neutron scattering by employing a combination of time-of-flight and backscattering techniques is carried out to explore the molecular mobility of a polymer of intrinsic microporosity (PIM-1) at microscopic time scales in comparison with a high-performance polyimide. Molecular fluctuations can change the structure of the temporary network of micropores and open or close pathways for gas molecules. Therefore, the investigation might help to understand the selectivity of PIMs in gas separation processes. The performed neutron scattering experiments provide evidence for a low-temperature relaxation process, which was assigned to methyl group rotation. This methyl group rotation was analyzed in terms of jump diffusion in a three-fold potential. The analysis results in a fraction of methyl groups which are immobilized. For PIM-1 it was found that the fraction of immobilized methyl groups decreases with increasing temperature up to 350 K. At higher temperatures the number of immobilized methyl group increases gain due to an underlying relaxation process. This motional process on a somewhat larger length scale might lead to a reversible structural rearrangement which partially hinders the strongly localized methyl group rotation. In addition, it was found that the activation energy for the methyl group rotation for PIM-1 and the polyimide is significantly higher than for conventional polymers.

KEYWORDS: Polymers of intrinsic microporosity, PIM-1, Quasielastic neutron scattering, Methyl group rotation: Permselectivity

MANUSCRIPT TEXT

1. Introduction

Polymers of intrinsic microporosity (PIMs) appeared as a new class of polymers about 16 years ago. PIMs have interconnected pores with characteristic sizes less than 2 nm and Brunauer–Emmett–Teller (BET) surface areas mostly larger than 700 m^2 g^{-1}. Most PIMs consist of uncrosslinked polymer chains, soluble in conventional solvents which enables easy processing. The contorted ladder-type backbone structure of PIMs leads to inefficient packing in the solid state.[1] Due to the unique structural features of PIMs, a variety of possible applications of them have been discussed. These applications include organic light emitting diodes (OLEDs) and sensors,[2-4] electrochemical devices[5-10] or membranes for pervaporation[11,12], and nanofiltration.[13] One of the most promising possible applications of PIMs is their use as active materials in membranes for gas separation processes.[14-16]The separation of gas mixtures is an integral part of many processes in the chemical industry and natural gas treatment, as well as biogas upgrading. The essential quantities characterizing materials for gas separation are the permeability P and the permselectivity α.[17,18] The latter is defined as the ratio of the permeabilities of two different gases.

$$\alpha_{ab} = \frac{P_a}{P_b} \qquad (1)$$

Based on experimental data of a large number of polymers, a limiting trade-off behaviour was observed between permselectivity and permeability for technically relevant gas pairs and published by Robeson in 1991[17-21] as the well-known upper-bound in a double-logarithmic plot of permselectivity α_{ab} vs. permeability of the more permeable gas P_a. Freeman [22,23] established a theoretical basis for these empirical relations.

While the solubility of a gas molecule in a certain polymer is mainly related to its the diffusivity depends on its effective size, i.e. the minimal diameter of the molecule allowing the passage through a rigid or dynamic bottleneck of the polymer matrix. For such consideration effective kinetic diameters obtained from measurements on zeolites were used.[19,24-26] Thus, the permselectivity of high-performance membrane polymers based on solution-diffusion is ascribed to a discrimination with respect to the effective diameter of the respective gas molecules.

When microporous structures are considered, also the general question concerning the transport mechanism arises which has been intensively discussed by Wijmans and Baker.[17,27] They postulate the

transition between Knudsen flow through pores and solution-diffusion in the fractional free volume of dense polymers at characteristic sizes in the range of 5 to 10 Å (0.5 -1 nm) but also emphasize that the temporal stability of the pore network is an essential factor for the transport mechanism.

PIMs are characterized by an outstandingly high permeability in combination with a still reasonable selectivity. The latter point is somehow surprising; because of the interconnected pore network a more Knudsen-like diffusion might be expected instead of a size-discriminating transport process. Concerning the size-dependence of gas diffusivities an analysis of data of PIMs and thermally rearranged (TR) polymers, a linear relation of diffusivity and the squared effective gas diameter is suggested.[28] A closer look at the respective plot reveals a slight deviation from this behavior for the smallest gases He and H_2 in PIM-1, which was proposed as being characteristic for several PIMs in a recent paper by Fuoco et al.[29] Their more detailed analysis shows that the diffusion of very small gas molecules like H_2 or He follows a much less pronounced linear size dependence compared to the larger gases O_2, CO_2, N_2 and CH_4. So, their behavior follows a characteristic known for porous materials like zeolites, rather than the behavior of conventional glassy polymers without microporosity. This was also shown as being distinctly different from the behavior of poly(1-trimethylsilyl-1-propyne) (PTMSP) also a rigid ultrapermeable polymer, which exhibits permeabilities in the same range as PIMs but with considerably lower selectivities. Moreover, the existence of characteristic bottlenecks was evidenced by molecular dynamics (MD) simulations. It is suggested that these bottlenecks form windows between individual free volume elements (parts of the microporosity) with variable sizes between the effective sizes of the smaller gases He and H_2 and the larger gases. So, the small gases can always pass these windows, whereas the passage of the larger gases is coupled with the dynamics of these characteristic bottlenecks, giving rise to the attractive selectivities of PIMs for membrane separations.

In that respect the molecular mobility of PIMs must be discussed. Due to molecular fluctuations, like the rotation of methyl groups, the bottlenecks between the free volume elements can be opened or closed. The molecular mobility of high-performance polymers has already been investigated by quasielastic neutron scattering.[30-32] It was concluded that molecular fluctuations at a time scale of picoseconds are relevant for the gas transport in polymers. Moreover, a correlation between the neutron data and the diffusion coefficient of gas molecules has been reported.[30]

The first synthesized polymer of intrinsic microporosity was PIM-1, a polybenzodioxane.[33,34] As for most other PIMs investigated since then, no glass transition temperature could be measured by conventional differential scanning calorimetry before the chemical decomposition of the polymer.[14] Recently fast scanning calorimetry was applied to study the glass transition of PIM-1.[35,36] By this approach the kinetics of chemical decomposition and glassy dynamics are decoupled and a glass transition temperature of 644 K at a heating rates of 10^4 K was estimated. When prepared as a film, from solution by slow evaporation of the solvent, they show an early solidification due to their rigid backbone and their limited molecular mobility. This gives rise to their microporosity resulting from inefficient packing, but also leads to strong physical aging effects which limits their application.[37] PIMs share this unwanted property with other glassy polymers like polyimides (see for instance [38,39,40]) or polynorbornenes with stiff main chains and bulky side groups.[41,42] In addition to fast scanning calorimetry, the molecular mobility PIM-1 was investigated by broadband dielectric spectroscopy.[43] A single relaxation process was observed at high temperatures with relaxation rates having an Arrhenius-like temperature dependence with an activation energy of 104 kJ/mol. This process designated as β*-relaxation was assigned to molecular fluctuations of aggregates. Recently inelastic neutron scattering was employed to study the vibrational density of states in the energy range of a few meV.[44] Characteristic excess vibrations (Boson Peak) to the Debye type density of states were found. Compared to the Boson Peak of conventional polymers, the Boson Peak for PIM-1 is shifted to lower frequencies. This was discussed in terms of a higher compressibility on a molecular length scale due to the sponge-like microporous structure of PIM-1. In the present study, quasielastic neutron scattering was applied to investigate the molecular mobility of PIM-1. A polymer with no intrinsic microporosity is included in the investigation to compare it with PIM-1. For that comparison, Matrimid was chosen as a commercially available high-performance polyimide. Matrimid has a fractional free volume of 13- 15 % and no intrinsic microporosity (i.e. no significant BET surface). It is frequently used in studies addressing the gas transport of gases or related problems.[38,39]

2. Experimental Section

Sample Preparation

The chemical structures of PIM-1 together with an optimized model of the repeat unit and Matrimid are shown in Figure 1a and 1b. The synthesis of PIM-1 was discussed in more detail in ref. 43. The molecular weight M_W was estimated as 82800 g/mol with a polydispersity index of 2.8 by size exclusion chromatography using chloroform as solvent and polystyrene as calibration standard. Matrimid 5218 was obtained from Huntsman International LLC. It was provided in the fully imidized state according to the producer.

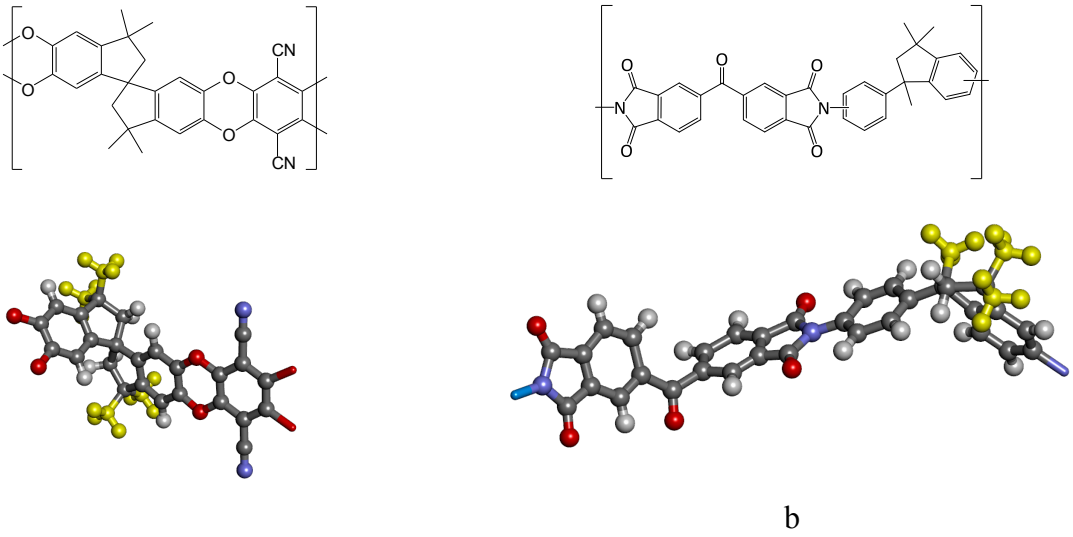

a b

Figure 1: Chemical structure of PIM-1 (a) and Matrimid (b).

Films were prepared from both polymers using the preparation conditions that were discussed in detail in ref. 43. In short, 1 g of the polymer was dissolved in chloroform with shaking for 4 to 5 hours, followed by ultra-sonication for 5 min. After that the solution was filtered employing a 5 µm PTFE-filter. To obtain a film the solution was cast in a Teflon mold. The mold was placed in a closed chamber where its atmosphere is saturated with chloroform to control the evaporation of the solvent from the film. In the literature, different annealing temperatures in the range from 40 °C to 100 °C have been employed, which result in different PIM-1 films having somewhat different gas permeability values.

Here, the films of both polymers were annealed at 100 °C (375 K) for 3 days after removing from the Teflon mold.

To minimize physical aging effects, the samples were prepared just before the measurement. For the neutron experiment the films were hermetically welded in flat aluminum cells which are transparent to neutrons.

Neutron Scattering

Inelastic neutron scattering is sensitive to molecular motions at microscopic length scales and times.[45] The experiments were carried out by different spectrometers working with different principles. Momentum and energy are exchanged between the nuclei of the sample and the neutrons. As the main experimental quantity, the double differential cross section is obtained which is given by

$$\frac{d^2\sigma}{d\Omega\, d\omega} = \frac{1}{4\pi}\frac{k_f}{k_i}\left(\sigma_{coh}S_{coh}(q,\omega) + \sigma_{inc}S_{inc}(q,\omega)\right) \qquad (2)$$

k_i and k_f are the incident and final wave vectors of the neutron beam, respectively, defining the scattering vector q. The measured energy transfer ΔE is related to the angular frequency ω by ω=ΔE/ħ. Ω is the solid angle of detection. σ_{coh} and σ_{inc} are the scattering cross-sections for coherent and incoherent scattering, where $S_i(q,\omega)$ are the coherent and incoherent dynamic structure factors (scattering functions). PIM-1 and Matrimid contain hydrogen (H), carbon (C), nitrogen (N), and oxygen (O) (see Figure 1) where the corresponding scattering cross-sections are given in Table 1. Hydrogen is the strongest (mostly incoherent) scatterer and the (mostly coherent) contributions of all nuclei for PIM-1 and Matrimid are much smaller. This means the measured scattering will be predominantly incoherent and due to the hydrogen nuclei.

Table 1: Cross-section for incoherent and coherent scattering of the relevant nuclei.

Nuclei	σ_{inc} [barn]	σ_{coh} [barn]
H	80.27	1.756

C	0	5.551
N	0.3	11.01
O	0	4.232

Elastic scans: Elastic fixed window scans (ΔE≈0) employing a neutron backscattering spectrometer provide an overview about the molecular dynamics at a time scale of ca. 2 ns. The corresponding measurements were carried out at the high-resolution spectrometer SPHERES[46,47] operated by the Jülich Centre for Neutron Science (JCNS) at the Heinz Maier-Leibnitz Zentrum (MLZ) in Garching, Germany. SPHERES is a cold neutron backscattering spectrometer of the third generation with focusing optics and a rotating phase-space-transform chopper. It was used in standard configuration with an incident wavelength of λ_n= 6.27 Å. The maximal accessible elastic scattering vector was q=1.76 Å^{-1}. An effective mean-square displacement $\langle u^2 \rangle_{eff}$ is calculated from the elastic scattered intensities. For that purpose, the usual Gaussian form

$$I_{el}(q)/\, I_0(q) = e^{(-q^2 \langle u^2 \rangle_{eff}/3)} \quad (3)$$

with the addition of a multiple-scattering contribution[48] was used (I_{el}(q) and I_0(q) are the elastically and totally scattered intensities). I_0(q) was estimated by a measurement with increased statistics at 10 K. The scans were carried out with a heating rate of 0.45 K/min, which corresponds to one data point per 0.5 K.

Quasielastic measurements: For the quasielastic neutron scattering, neutron time-of-flight spectroscopy was combined with neutron backscattering spectroscopy. This combination results in a broad time range. The multi-chopper cold neutron time-of-flight spectrometer TOFTOF[49] was employed for the time-of-flight measurements. It is operated by the Technische Universität München at the MLZ. TOFTOF was used employing a standard configuration with an incident wavelength of λ_n= 6 Å. This results in an energy resolution 45…62 μeV (full width at half maximum (FWHM), increasing with higher scattering angle) with a maximal accessible elastic scattering vector of q=2.3 Å^{-1}. The incoherent dynamic structure factor for PIM-1 measured at TOFTOF for different temperatures is depicted in

Figure 2a. The spectra measured for higher temperatures show the characteristic quasielastic broadening compared to the resolution of the spectrometer measured at 4 K.

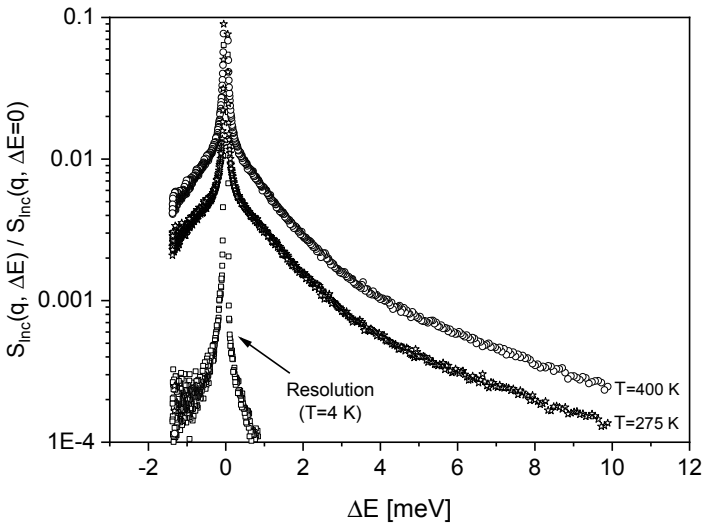

Figure 2a: Neutron Time-of-Flight spectra measured at TOFTOF for PIM-1 at the indicated temperatures at a q vector of 1.42 $Å^{-1}$. The spectra were normalized by the peak value of the elastic line. The scattering of the empty can is already subtracted. The statistics of the measurement can be judged from the scatter of the data.

Neutron backscattering was carried out at the backscattering spectrometer SPHERES (see above). SPHERES was again used in standard configuration with an incident wavelength of λ_n= 6.27 Å and an average resolution of 0.59 μeV (FWHM). Figure 2b depicts $S_{Inc}(q, \Delta E)$ for PIM-1 measured at SPHERES for different temperatures. The neutron backscattering spectra also show the characteristic quasielastic broadening.

The resolutions for both instruments R(q,ΔE) were obtained by measuring the sample at 4 K. It is assumed that all molecular fluctuations leading to quasielastic scattering are frozen besides quantum zero-point motions. The program INX[50] was used to evaluate the TOFTOF data. It features TOF to energy conversion, background subtraction, vanadium normalization, and self-attenuation correction. The neutron backscattering data measured with SPHERES were analyzed by the program SQW.[51] SQW applies backscattering and vanadium normalization, self-attenuation correction, and in addition

performs an attenuation correction on the background to be subtracted. Both programs calculate an effective but cross section weighted $S_{Inc}(q,\Delta E)$.

The time-of-flight and the backscattering data have a large difference in the energy resolution (see Figure 2). Therefore, both sets of data were Fourier transformed and divided by the Fourier transform of the corresponding resolution. Hereby absolute values of the incoherent intermediate scattering function $S_{Inc}(q,t)$ were obtained. In that way, the data from time-of-flight and backscattering can be jointly analyzed in the time domain. Moreover, both data sets were corrected for multiple scattering. For that a procedure working in time domain was employed.[52] The multiple scattering fraction was fitted to optimize the limit $S_{inc}(q\rightarrow 0,t)=1$ because the exact scattering geometry is not known. With respect to single scattering the estimated multiple scattering fractions for PIM-1 were 19% and 22% for SPHERES and TOFTOF respectively and for Matrimid 18% and 16%.

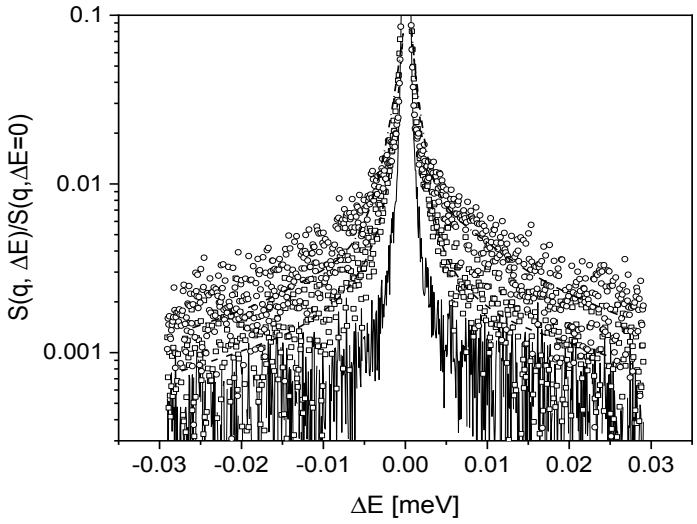

Figure 2b: Neutron backscattering spectra from SPHERES for PIM-1 at an angle of 90°. The spectra were normalized by the peak value of the elastic line. The scattering of the empty cell is already subtracted. Thin solid line – 4 K (resolution), squares – 200 K and circles – 300 K. The thick dashed line is a guide to the eyes for the data at 200 K and the dashed dotted line is a guide to the eyes for the data at 300 K. The statistics of the measurement can be judged from the scatter of the data.

3. Results and Discussion

Figure 3a depicts the temperature dependence of the effective mean squared displacement for PIM-1 and Matrimid. For low temperatures, the temperature dependence of the effective mean squared displacement from both materials is due to vibrations. In addition, for PIM-1 a clear step-like change in $\langle u^2_{eff} \rangle(T)$ in the temperature range from 100 K and 250 K occurs, indicating the onset of molecular fluctuations at a time scale of ca. 1 ns. By means of dielectric spectroscopy no relaxation process was observed for PIM-1 in this temperature range.[43] This means the fluctuations detected by the elastic scan must be due to fluctuations of nonpolar groups. The only moieties which can be mobile at this low temperature are the methyl groups. Therefore, the detected process is assigned to the methyl group rotation. Nevertheless, it is known from the literature that for conventional polymers the methyl group rotation is observed in the temperature range of 100 und 150 K at a time scale of ca. 1 ns.[53,54] When the point of inflection in $\langle u^2 \rangle_{eff}$ appears at a higher temperature a higher thermal energy is need to activate the underlying process. Therefore, this points to a higher activation energy for the methyl group rotation of PIM-1 and the high-performance Matrimid in comparison to conventional polymers.

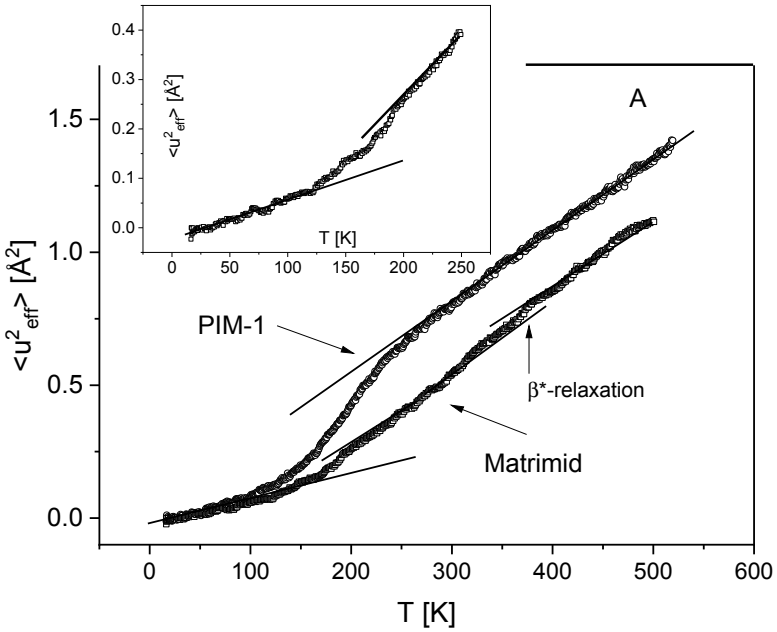

Figure 3a: Effective mean squared displacement $\langle u^2_{eff} \rangle$ versus temperature: circles – PIM-1, squares – Matrimid. The inset enlarges the low temperature range for Matrimid. For Matrimid the position of the β^*-relaxation observed by dielectric spectroscopy is indicated.[55]

Lines are guides for the eyes.

For Matrimid also a change in the temperature dependence of the effective mean squared displacement is detected. However the observed change in $\langle u^2_{eff} \rangle(T)$ for Matrimid is much smaller than that observed for PIM-1 (see Figure 3a, and inset of Figure 3a). At first glance one must consider that PIM-1 has 4 methyl groups while Matrimid has only 3. In the case that the number of methyl groups per repeat unit is the only difference between the processes in both polymers a scaling by SF= (3 * number of methyl groups) / (number of all protons in the repeating unit) should lead to an overlap of the mean squared displacement for both polymers. Figure 3b shows that the curves collapse in their onset consistent with the interpretation of methyl group rotation as the molecular origin. Nevertheless, the point of inflection in $\langle u^2 \rangle_{eff}(T)$ is shifted to a higher temperature for Matrimid, indicating a difference in the thermal activation. Moreover, at temperatures >200 K, $\langle u^2 \rangle_{eff}(T)$ increases more strongly than expected, probably due to the onset of the β*-relaxation for Matrimid.

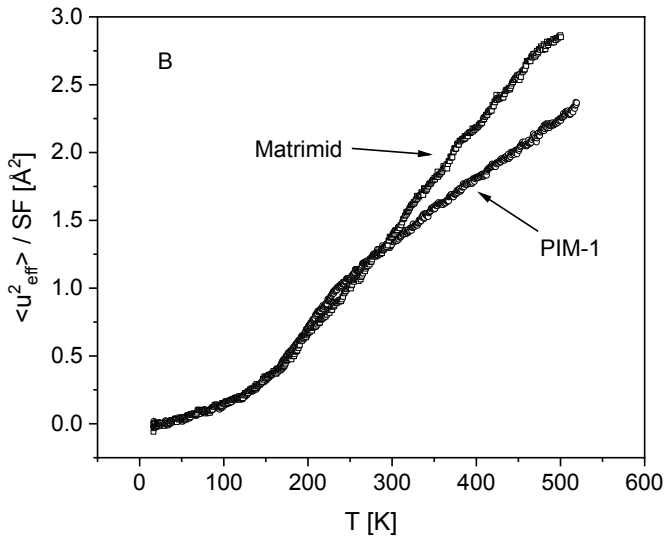

Figure 3b: Effective mean squared displacement $\langle u^2_{eff} \rangle$ versus temperature normalized by the scaling factor described in the text: circles – PIM-1, squares – Matrimid.

In addition to the elastic scans, the molecular mobility of PIM-1 and Matrimid was also investigated by quasielastic neutron scattering. Figure 4 gives the incoherent intermediate (time dependent) scattering function $S_{Inc}(q,t)$ at 300 K for different q-vectors. The data in the range from 0.1 ps to 30 ps corresponds to neutron time-of flight measurements at TOFTOF while the data from 30 ps to ca. 3 ns were measured

by neutron backscattering on SPHERES. Both data sets match together. $S_{Inc}(q,t)$ shows a single decay indicating a relaxation process which is assigned to methyl group rotation. For Matrimid a corresponding behavior is observed. The standard model for methyl group rotation is the Rotation Rate Distribution Model (RRDM).[53] In our treatment for simplicity a stretched exponential function is fitted to the data

$$S_{Inc}(q,t) = DWF * \left((1 - EISF_M) \exp\left(-\left(\frac{t}{\tau_M}\right)^{\beta_M} \right) + EISF_M \right), \quad (4)$$

where DWF is the Debye-Waller factor, τ_M is the relaxation time for methyl group rotation and β_M is the stretching parameter describing the distribution of relaxation times. $EISF_M$ denotes the Elastic Incoherent Structure Factor.

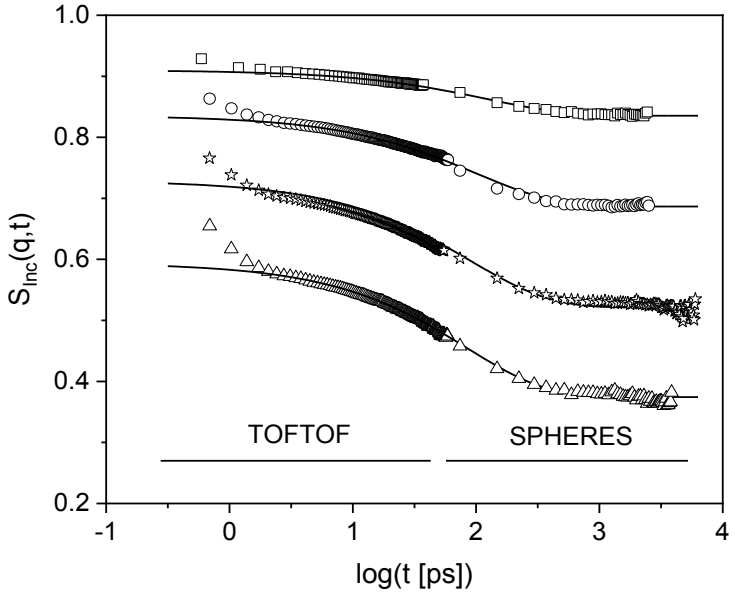

Figure 4: Incoherent intermediated scattering function $S_{Inc}(q,t)$ versus time for PIM-1 for different q vectors at 300 K: squares – 0.69 $Å^{-1}$, circles – 1.04 $Å^{-1}$, asterisk – 1.42 $Å^{-1}$ and triangles – 1.76 $Å^{-1}$.

The data can be well described by Equ. 4. (Values of β_M are given in the supporting information.) The Elastic Incoherent Structure Factor for the methyl group rotation can be calculated in the framework of

jump rotation in a threefold potential $V(\phi) \sim (1 - \cos(3\phi))/2$ which is the most straightforward model for methyl group rotation.[53,56] It results from the three equivalent energy minima with respect to the rotation angle ϕ of the methyl group. Within this model $EISF_M$ is given by

$$EISF_M(q) = \frac{1}{3}\left(1 + 2\frac{\sin(\sqrt{3}\,qr)}{\sqrt{3}\,qr}\right) \quad (5)$$

r is the radius of the circle spanned by the positions of the hydrogen nuclei of the methyl group which is 1.027 Å. In Figure 5a and 5b the q dependence of the $EISF_M$ for PIM-1 and Matrimid in comparison to the calculation of Equ. 5 is depicted. The calculated data do not agree with the experimental values.

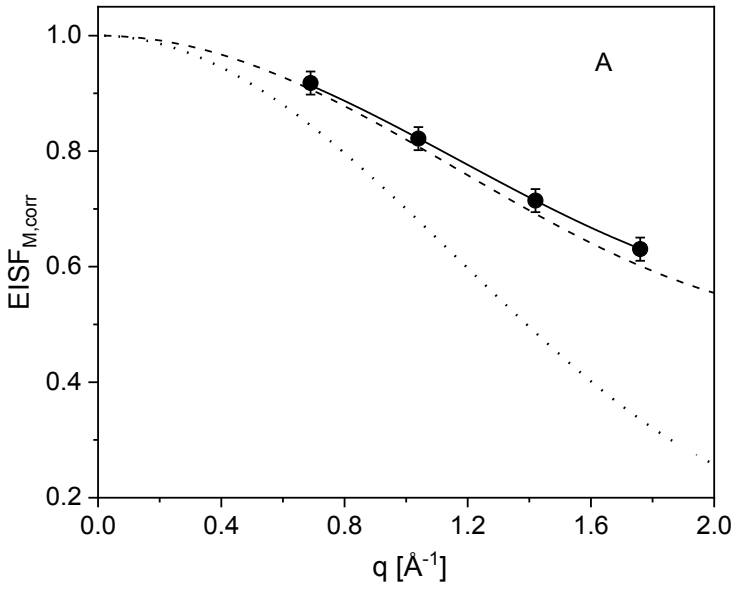

Figure 5a: q dependence of the elastic incoherent structure factor for PIM-1 at T=300 K. Dotted line - calculated data according to Equ. 5. Dashed line - calculated data according to Equ. 6 with the theoretical value of C_{fix}=0.4. Solid line fit of Equ. 6 to the data. Typical error bars are estimated based on the errors of the fits of Equ. 4.

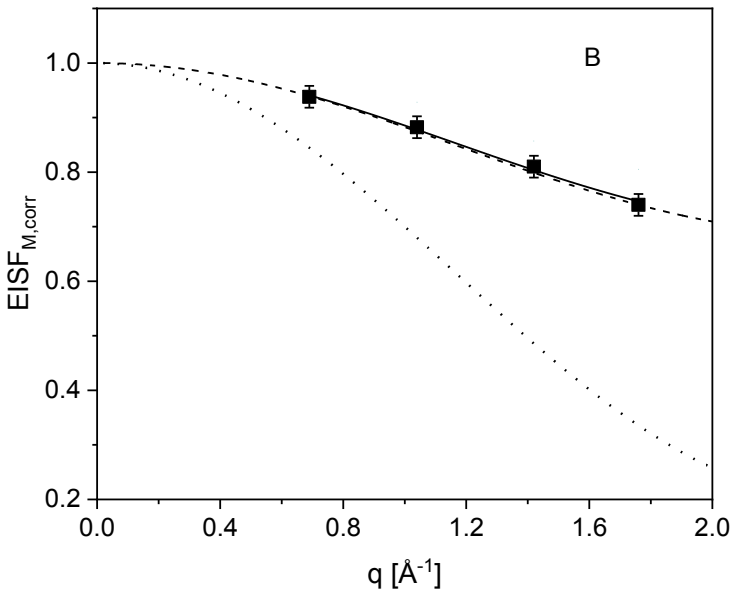

Figure 5b: q dependence of the elastic incoherent structure factor for Matrimid at T=300 K. Dotted line - calculated data according to Equ. 5. Dashed line - calculated data according to Equ. 6 with the theoretical value of C_{fix}=0.6086. Solid line fit of Equ. 6 to the data. Typical error bars are estimated based on the errors of the fits of Equ. 4.

To discuss the discrepancy of the theoretical data and the experimental values one must consider that for both PIM-1 and Matrimid not all hydrogen nuclei are in the methyl groups. For PIM-1 20 hydrogen nuclei are in the repeat unit of which 12 protons are in the methyl groups. This means 8 protons do not participate in the methyl group rotation and scatter elastically at the considered temperature far below T_g. The fraction of elastic scattering hydrogen nuclei C_{fix} is 0.4. For Matrimid 9 of 23 protons are in methyl groups. This means 14 hydrogen nuclei scatter elastically (C_{fix}=0.6086). With these considerations Equ. 5 must be corrected for elastic scattering to[52,54,57]

$$\mathrm{EISF_{M,corr}}(q) = (1 - \mathrm{C_{fix}})\mathrm{EISF_M}(q) + \mathrm{C_{fix}}. \qquad (6)$$

Figure 5b shows that this approach works quite well with the theoretical fraction C_{fix} for Matrimid. For PIM-1 a systematic deviation of the calculated from experimental values is observed. For that reason, Equ. 6 is fitted to the experimental data and effective values of C_{fix} are estimated from that as function of temperature. Figure 6 shows C_{fix} normalized to the theoretical value $C_{fix,\,theoretical}$ for PIM-1 and Matrimid. For

Matrimid C_{fix} is close to the theoretical value. This good agreement indicates that the observed process is indeed the methyl group rotation. The significantly lower value obtained for T=400 K is probably due to contributions of protons not belonging to the methyl groups and becoming mobile above the β*-relaxation of Matrimid which has been identified earlier in the temperature range above 350 K.[55] Also a corresponding change in the effective mean squared displacement for Matrimid is observed in this temperature range (see Figure 3a).

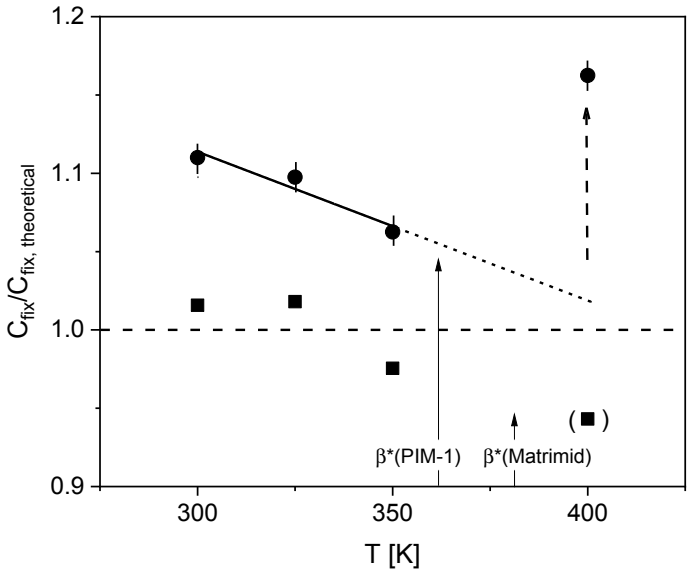

Figure 6: Fraction of immobilized hydrogen nuclei normalized by the theoretical fraction: circles – PIM-1, squares – Matrimid. The dashed line represents the theoretical fraction. Typical error bars are estimated based on the errors of the fits of Equ. 4.

For PIM-1 a different behavior is observed. In general, C_{fix} is higher than the theoretical value, i.e. a part of the methyl groups is somewhat immobilized. Furthermore, C_{fix} decreases with increasing temperature indicating that the number of mobile methyl groups increases due to a change in the microporous structure with increasing temperature. An extrapolation of this trend yields that at 400 K the theoretical value is reached. Surprisingly, the experimental value of the immobilized methyl groups at 400 K is distinctly increased. (Unfortunately, experiments at higher temperatures cannot be carried out because PIM-1 will undergo significant physical aging during the prolonged time-period needed for a backscattering experiment at one temperature.) At first it seems reasonable to ascribe this to structural changes resulting from aging processes. But this increase of C_{fix} cannot be explained by physical aging,

which would be irreversible, because a second elastic scan carried out after the first one (not shown here) gives identical data. As mentioned above, dielectric investigations performed earlier on PIM-1 evidence one relaxation process called β*-relaxation becoming active at temperatures above 350 K.[43] This relaxation process has a rather high activation energy above 80 kJ/mol and is therefore assigned to coordinated fluctuations of aggregates. The the molecular origin of the β*-relaxation for PIM-1 is essential different from that of Matrimid. For a detailed discussion see ref. 43. At the first glance this β*-relaxation is not manifest in the temperature dependence of the mean squared displacement from the neutron scattering results for PIM-1. For that reason, $\langle u^2_{eff} \rangle$(T) is analyzed in more detail in the temperature range above the methyl group rotation (see Figure 7). In order to visualize the change in the slope in $\langle u^2_{eff} \rangle$(T) we fitted linear functions in the ranges 250...300 K and 400...525 K, respectively. With this procedure we do not want to imply that $\langle u^2_{eff} \rangle$(T) has to follow a linear behavior in general.

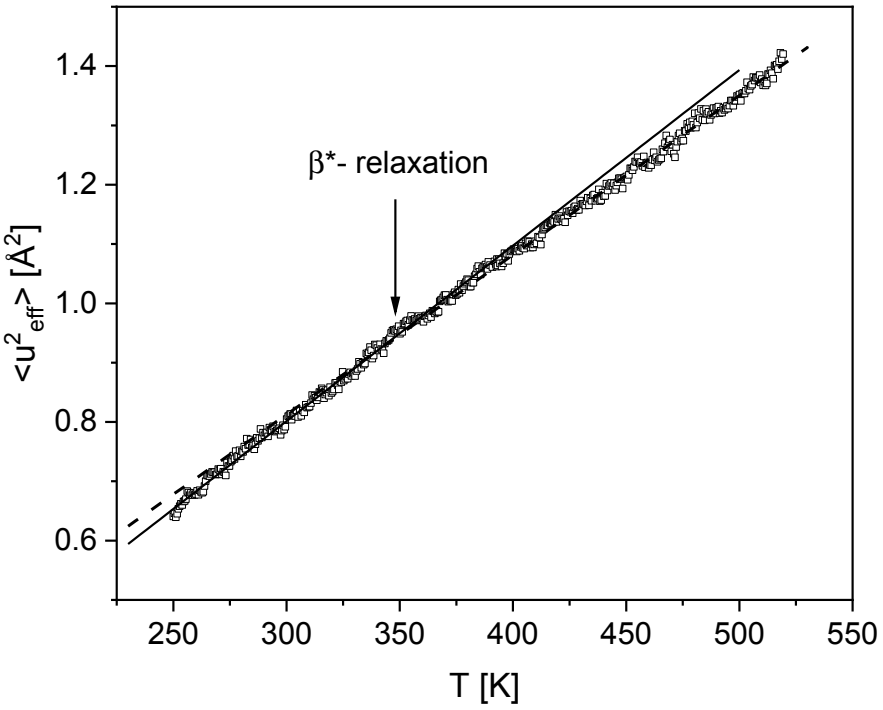

Figure 7: Temperature dependence of the effective mean squared displacement in the temperature range from 250 K and 525 K. The solid line is a linear fit to the data in the temperature range from 250 K to 350 K. Dashed line linear regression to the data in the

temperature range above 400 K.

The slopes of both fit lines are significantly different and the transition between both lines is in the temperature range around 350 K where the β*-relaxation becomes active. The slope in the high temperature range is lower than in the low temperature range indicating some immobilization. Therefore, it is concluded that the β*-relaxation of PIM-1 might be the reason for the sudden increase of C_{fix} indicating the immobilization of a part of the methyl groups.

As expected for a localized process like methyl group rotation, the relaxation time does not depend on the q vector (see supporting information).

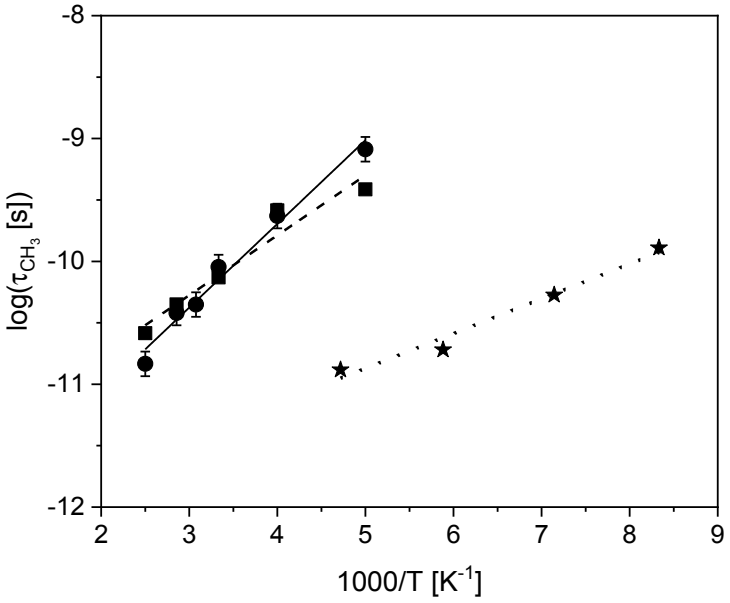

Figure 8: Relaxation time for methyl group rotation versus inverse temperature for q=1.76 Å^{-1}: circles – PIM-1, squares – Matrimid, asterisks – poly(methyl phenyl siloxane). The data for the poly(methyl phenyl siloxane) were taken from reference 54. Lines are fits of the Arrhenius equation to the data. Typical error bars are estimated based on the errors of the fits of Equ. 4.

Figure 8 gives the temperature dependence of the relaxation time versus inverse temperature (relaxation map) for PIM-1 and Matrimid. Moreover, data for the conventional polymer poly(methyl phenyl siloxane) are included for comparison. This comparison shows that the methyl group dynamics for PIM-1 and Matrimid is shifted to higher temperature. This is due to the higher steric hindrance of the methyl

group rotation because of the stiff and rigid chain structure of PIM-1 and Matrimid. The temperature dependence of the relaxation time of methyl group rotation follows the Arrhenius equation which reads

$$\tau_{CH_3} = \tau_\infty \exp\left(\frac{E_A}{RT}\right) \quad (7)$$

where E_A is the activation energy, τ_∞ is the relaxation rate at infinite temperatures, and R is the universal gas constant. The Arrhenius equation is fitted to the data and the activation energies are estimated as 13 kJ/mol for PIM-1, 9 kJ/mol for Matrimid, and 5.4 kJ/mol for poly(methyl phenyl siloxane). (Further values of the activation energies for the methyl group ration of other conventional polymers like PMMA can be found elsewhere.[52,53] The values are in the same range as for poly(methyl phenyl siloxane).) The activation energies for PIM-1 and Matrimid are essentially higher than that of poly(methyl phenyl siloxane). This can be attributed again to the stiff and rigid chain structure of the high-performance polymers PIM-1 and Matrimid. Moreover, the activation energy for methyl group rotation is higher for PIM-1 than for Matrimid. This result might be understood by the more rigid chain structure of PIM-1 in comparison to Matrimid. This conclusion should be confirmed by further experimental investigations for instance on addition type polynorbornenes with bulky side groups and atomistic molecular dynamic simulations.

4. Conclusion

Quasielastic neutron scattering has been employed to investigate the molecular mobility of the high-performance polymer PIM-1. PIM-1 is a polymer of intrinsic microporosity with possible applications in gas separation membranes and electronics. Matrimid was chosen as reference material. The investigation was carried out to shed some light on the selectivity of polymers of intrinsic microporosity in gas separation processes. Molecular fluctuations like methyl group rotations can change the structure of the temporary interconnected microporous network and can open and close channels/bottlenecks between pores for gas transport processes. This statement does not mean that that the rate of the methyl group rotation directly correlates with the rate of the diffusion. Actually, for PIM-1 the rate of diffusion as well as gas solubility are mainly due to its microporosity which is not present in Matrimid. Therefore, the permeability is much higher for PIM-1 than for Matrimid. Values of the diffusion coefficients for different gases are compared for PIM-1 and Matrimid in the supporting information. It is reasonable to

assume that the gas diffusivity in Matrimid is determined primarily by motional processes on a larger length scale and the methyl group rotation does not play a significant role in that context. In contrast to that the transport properties of PIM-1 are dominated by its microporosity and continuous void phase. In this context the methyl group rotation may exert a relevant influence and thus affect the transport of gas molecules of different size in terms of selectivity It should be further noted that the role of the methyl groups the for physical aging of PIM-1 and its composites have also been discussed based on results obtained by NMR techniques.[58]

To gain an overview about the molecular dynamics, elastic scans were carried out. The effective mean squared displacement indicates one relaxation process which is assigned to the methyl group rotation in both polymers. A combination of neutron time-of-flight and neutron backscattering spectroscopy is used to investigate the methyl group dynamics in detail. To analyze time-of-flight and backscattering data together, the dynamic structure factors are Fourier transformed and divided by the Fourier transform of the corresponding resolution. This procedure results in absolute values of the incoherent intermediate scattering function $S_{Inc}(q,t)$. With this method a broad dynamical range can be covered by neutron scattering. $S_{Inc}(q,t)$ shows a single step-like decay which is further analyzed by a stretched exponential. As results, the relaxation time and the elastic incoherent static factor are obtained. The q dependence of the EISF is analyzed in terms of diffusional jump rotation in a threefold potential where the hydrogens which are not located in methyl groups are considered. For PIM-1 it was found that the fraction of mobile groups first increases with increasing temperature up to 350 K. At 400 K the number of mobile methyl groups is decreased again, which is discussed in the framework of the β*-relaxation found by dielectric spectroscopy. The temperature dependence of the relaxation time of the methyl group rotation follows the Arrhenius equation. The estimated activation energies of the methyl group rotation for PIM-1 and Matrimid are essentially higher than for a conventional polymer. This can be explained by the rigid and stiff backbone structures of PIM-1 and Matrimid. Moreover, the activation energy for the methyl group is higher for PIM-1 than for Matrimid.

It seems reasonable that the methyl group rotation and its complex interplay with the β*-relaxation affects the interconnected network of micropores and therefore might be an important aspect of the unusual transport behavior of PIMs giving rise to their extraordinary potential for gas separation membranes.

ASSOCIATED CONTENT

Supporting Information The Supporting Information is available free of charge at https://pubs.acs.org/doi/10.1021/acs.macromolxxxx

Values of the fit parameter β_M, q-dependence of the relaxation time τ_M; table of values of the diffusion coefficient for different gasses for PIM-1 and Matrimid

Corresponding Author

A. Schönhals, Bundesanstalt für Materialforschung und -prüfung (BAM), Unter den Eichen 87, 12205 Berlin, Germany; Email: Andreas.Schoenhals@bam.de

Authors contributions

AS initiated the work, RZ and AS carried out the measurements and all the data analysis, WJH and PMB synthesized PIM-1, MB significantly contribute the discussion. The manuscript was written by contributions of all authors. All authors have given approval to the final version of the manuscript.

Notes

The authors declare no competing financial interest.

Acknowledgements

The Heinz Maier-Leibnitz Zentrum (Garching/Germany) is thanked for enabling the neutron scattering experiments. Mr. Th. Rybak and Dr. H. Yin are thanked for their help with the sample preparation. Prof. Dr. Y. Yampolskii is grateful acknowledged for providing diffusions coefficients for PIM-1 and Matrimid for different gases. W. J. Harrison was supported by EPSRC grant EP/K016946/1 "Graphene-based membranes"

REFERENCES

1 Dawson, R.; Cooper, A. I.; Adams, D. J. Nanoporous Organic Polymer Networks. *Prog. Polym. Sci.* **2012**, 37, 530-563.
2 Gupta, B. K.; Kedawat, G.; Kumar, P.; Rafiee, M. A.; Tyagi, P.; Srivastava, R.; Ajayan, P. M. An n-type, New Emerging Luminescent Polybenzodioxane Polymer for Application in Solution-Processed Green Emitting OLEDs. *J. Mater. Chem. C* **2015**, 3, 2568-2574.
3 Gupta, B. K.; Kedawat, G.; Kumar, P.; Rafiee, M. A.; Tyagi, P.; Srivastava, R.; Ajayan, P. M. An n-type, New Emerging Luminescent Polybenzodioxane Polymer for Application in Solution-Processed Green Emitting OLEDs. *J. Mater. Chem. C* **2015**, 3, 2568-2574.
4 Rakow, N. A.; Wendland, M. S.; Trend, J. E.; Poirier, R. J.; Paolucci, D. M.; Maki, S. P.; Lyons, C. S.; Swierczek, M. J. Visual Indicator for Trace Organic Volatiles. *Langmuir* **2010**, 26, 3767-3770.
5 Ward, A. L.; Doris, S. E.; Li, L.; Hughes, M. A.; Qu, X.; Persson, K. A.; Helms, B. A. Materials Genomics Screens for Adaptive Ion Transport Behavior by Redox-Switchable Microporous Polymer Membranes in Lithium–Sulfur Batteries. *ACS Central Science* **2017,** 3, 399-406.
6 Xia, F.; Pan, M.; Mu, S.; Malpass-Evans, R.; Carta, M.; McKeown, N. B.; Attard, G. A.; Brew, A.; Morgan, D. J.; Marken, F. Polymers of Intrinsic Microporosity in Electrocatalysis: Novel Pore Rigidity Effects and Lamella Palladium Growth. *Electrochim. Acta* **2014,** 128, 3-9.
7 He, D.; Rauwel, E.; Malpass-Evans, R.; Carta, M.; McKeown, N. B.; Gorle, D. B.; Anbu Kulandainathan, M.; Marken, F. Redox Reactivity at Silver Microparticle - Glassy Carbon Contacts Under a Coating of Polymer of Intrinsic Microporosity (PIM). *J. Solid State Electrochem.* **2017,** 21, 2141-2146.
8 He, D.; Rong, Y.; Kou, Z.; Mu, S.; Peng, T.; Malpass-Evans, R.; Carta, M.; McKeown, N. B.; Marken, F. Intrinsically Microporous Polymer Slows Down Fuel Cell Catalyst Corrosion. *Electrochem. Commun.* **2015,** 59, 72-76.
9 Rong, Y.; Malpass-Evans, R.; Carta, M.; McKeown, N. B.; Attard, G. A.; Marken, F. High Density Heterogenisation of Molecular Electrocatalysts in a Rigid Intrinsically Microporous Polymer Host. *Electrochem. Commun.* **2014,** 46, 26-29.
10 Yang, Z.; Guo, R.; Malpass-Evans, R.; Carta, M.; McKeown, N. B.; Guiver, M. D.; Wu, L.; Xu, T. Highly Conductive Anion-Exchange Membranes from Microporous Tröger's Base Polymers. *Angew. Chem. Int. Ed.* **2016,** 55, 11499-11502.
11 Gao, L.; Alberto, M.; Gorgojo, P.; Szekely, G.; Budd, P. M. High-Flux PIM-1/PVDF Thin Film Composite Membranes for 1-butanol/Water Pervaporation. *J. Membr. Sci.* **2017**, 529, 207-214.
12 Adymkanov, S. V.; Yampolskii, Y. P.; Polyakov, A. M.; Budd, P. M.; Reynolds, K. J.; McKeown, N. B.; Msayib, K. J. Pervaporation of Alcohols Through Highly Permeable PIM-1 Polymer Films. *Polym. Sci. Ser. A* **2008,** 50, 444-450.

13 Gorgojo, P.; Karan, S.; Wong, H. C.; Jimenez-Solomon, M. F.; Cabral, J. T.; Livingston, A. G. Ultrathin Polymer Films with Intrinsic Microporosity: Anomalous Solvent Permeation and High Flux Membranes. *Adv. Funct. Mater.* **2014**, 24, 4729-4737.
14 Budd, P. M.; Elabas, E. S.; Ghanem, B. S.; Makhseed, S.; McKeown, N. B.; Msayib, K. J.; Tattershall, C. E.; Wang, D. Solution-Processed, Organophilic Membrane Derived from a Polymer of Intrinsic Microporosity. *Adv. Mater. (Weinheim, Ger.)* **2004**, 16, 456-459.
15 Rose, I.; Carta, M.; Malpass-Evans, R.; Ferrari, M.-C.; Bernardo, P.; Clarizia, G.; Jansen, J. C.; McKeown, N. B. Highly Permeable Benzotriptycene-Based Polymer of Intrinsic Microporosity. *ACS Macro Lett.* **2015,** 4, 912-915.
16 Carta, M.; Malpass-Evans, R.; Croad, M.; Rogan, Y.; Jansen, J. C.; Bernardo, P.; Bazzarelli, F.; McKeown, N. B. An Efficient Polymer Molecular Sieve for Membrane Gas Separations. *Science* **2013,** 339, 303-307.
17 Baker, R. W., Membrane Technology and Applications. John Wiley & Sons: Chichester, UK, 2004.
18 Yampolskii, Y. Polymeric gas separation membranes *Macromolecules* **2012**, 45, 3298-3311.
19 Robeson, L. M. The upper bound revisited. *J. Membr. Sci.* **2008**, 320, 390-400.
20 Swaidan, R.; Ghanem, B.; Pinnau, I. Fine-Tuned Intrinsically Ultramicroporous Polymers Redefine the Permeability/Selectivity Upper Bounds of Membrane-Based Air and Hydrogen Separations. *ACS Macro Lett.* **2015**, 4, 947-951.
21 Comesaña-Gándara, B.; Chen, J.; Bezzu, C. G.; Carta, M.; Rose, I.; Ferrari, M.-C.; Esposito, E.; Fuoco, A.; Jansen, J. C.; McKeown, N. B. Redefining the Robeson upper bounds for CO_2/CH_4 and CO_2/N_2 separations using a series of ultrapermeable benzotriptycene-based polymers of intrinsic microporosity, *Energy. Environm. Sci.*, **2019**, *12*, 2733-2
22 Freeman, B. D. Basis of permeability/selectivity tradeoff relations in polymeric gas separation membranes. *Macromolecules* **1999**, 32, 375-380.
23 Robeson, L. M.; Freeman, B. D.; Paul, D. R.; Rowe, B. W. An empirical correlation of gas permeability and permselectivity in polymers and its theoretical basis. *J. Membr. Sci.* **2009**, 341, 178-185.
24 Breck, D. W. Zeolite Molecular Sieves: Structure, Chemistry, and Use. J. Wiley & Sons: New York, 1974.
25 Teplyakov, V.; Meares, P. Correlation aspects of the selective gas permeabilities of polymeric materials and membranes *Gas Separation & Purif.* **1990**, 4, 66-74.
26 Robeson, L. M.; Smith, Z. P.; Freeman, B. D.; Paul, D. R. Contributions of diffusion and solubility selectivity to the upper bound analysis for glassy gas separation membranes *J. Membr. Sci.* **2014**, 453, 71-83.
27 Wijmans, J. G.; Baker, R. W., The solution-diffusion model: a review. *J. Membr. Sci.* **1995**, 107, 1-21.
28 Robeson, L. M.; Dose, M. E.; Freeman, B. D.; Paul, D. R., Analysis of the transport properties of thermally rearranged (TR) polymers and polymers of intrinsic microporosity (PIM) relative to upper bound performance. *J. Membr. Sci.* **2017**, 525, 18-24.
29 Fuoco, A.; Rizzuto, C.; Tocci, E.; Monteleone, M.; Esposito, E.; Budd, P. M.; Carta, M.; Comesañ-Gándara, B.; McKeown, N. B.; Jansen, J. C. The origin of size-selective gas transport through polymers of intrinsic microporosity *Journal of Materials Chemistry A* **2019**, 7, 20121-20126
30 Inoue, R.; Kanaya, T.; Masuda, T.; Nishida, K.; Yamamuro, O. Relationship between the Local Dynamics and Gas Permeability of Para-Substituted Poly(1-chloro-2-phenylacetylenes) *Macromolecules* **2012**, 45, 6008-6014.
31 Kanaya, T.; Teraguchi, M.; Masuda, T.; Kaji, K. Local mobility of substituted polyacetylenes measured by quasielastic neutron scattering and its relationship with gas permeability *Polymer* **1999**, 40, 7157−7161.

32 T.; Kawaguchi, T.; Kaji, K. Role of Local Dynamics in the Gas Permeability of Glassy Substituted Polyacetylenes. A Quasielastic Neutron Scattering Study *Macromolecules* **2002**, 35, 5559−5564.
33 Budd, P.M.; Ghanem, B. S.; Makhseed, S.; McKeown, N. B.; Msayib, K. J.; Tattershall, C. E. Polymers of intrinsic microporosity (PIMs): robust, solution-processable, organic nanoporous *Chem. Commun. (Cambridge, U. K.)*, **2004**, **0**, 230-231.
34 Budd, P. M.; Msayib, K. J.; Tattershall, C. E.; Ghanem, B. S.; Reynolds, K. J.; McKeown, N. B.; Fritsch, D. Gas separation membranes from polymers of intrinsic microporosity *J. Membr. Sci.*, **2005**, 251, 263-269.
35 Yin, H.; Chua, Y. Z.; Yang, B.; Schick, C.; Harrison, W. J.; Budd, P. M.; Böhning, M.; Schönhals, A. First Clear-Cut Experimental Evidence of a Glass Transition in a Polymer with Intrinsic Microporosity: PIM-1. *J. Phys. Chem. Lett.* **2018,** 9, 2003-2008.
36 Yin, H.; Yang, B.; Chua, Y. Z.; Szymoniak, P.; Carta, M.; Malpass-Evans, R.; McKeown, Harrison, W. J.; Budd, P. M. Schick, C.; Böhning, M.; Schönhals, A. Effect of Backbone Rigidity on the Glass Transition of Polymers of Intrinsic Microporosity Probed by Fast Scanning Calorimetry *ACS Macro Letters* **2019**, 8,1022-1028.
37 Budd, P. M.; McKeown, N. B.; Ghanem, B. S.; Msayib, K. J.; Fritsch, D.; Starannikova, L.; Belov, N.; Sanfirova, O.; Yampolskii, Y.; Shantarovich, V. Gas permeation parameters and other physicochemical properties of a polymer of intrinsic microporosity: Polybenzodioxane PIM-1 *J. Membr. Sci.* **2008**, 325, 851-860.
38 Bos, A.; Pünt, I. G. M.; Wessling, M.; Strathmann, H. Plasticization-resistant glassy polyimide membranes for CO_2/CO_4 separations *Sep. Purif. Technol.* **1998**, 14, 27-39.
39 Simmons, J. W.; Ekiner, O. M. Polyimide and polyamide-imide gas separation membranes 1993, US5232472 A.
40 Konnertz, N; Böhning, M.; Schönhals, A. Dielectric investigations of nanocomposites based on Matrimid and Polyhedral Oligomeric Phenethyl-Silsesquioxanes (POSS) *Polymer*, **2016**, 90, 89-101.
41 Yin, H.; Chapala, P.; Bermeshev, M.; Schönhals, A.; Böhning, M. Molecular mobility and physical aging of a highly permeable glassy polynorbornene as revealed by dielectric spectroscopy *ACS Macro Lett.* **2017**, 6, 813-818.
42 Yin, H.; Chapala, P.; Bermeshev, M.; Pauw, B. R.; Schönhals, A.; Böhning. M. Influence of trimethylsilyl side groups on the molecular mobility and charge transport in highly permeable glassy polynorbornenes ACS Applied Polymer Materials **2019**, 1, 844-855.
43 Konnertz, N.; Ding Y.; Harrison, J W; Budd, P. M.; Schönhals. A; Böhning, M. Molecular mobility of the high performance membrane polymer PIM-1 as investigated by dielectric spectroscopy *ACS Macro Lett.*, **2016**, 5, 528-532.
44 Zorn, R.; Yin, H.; Lohstroh, W.; Harrison, W.; Budd, P. M.; Pauw, B. R.; Böhning, M.; Schönhals, A. Anomalies in the low frequency vibrational density of states for a polymer with intrinsic microporosity – the Boson peak of PIM-1 *Physical Chemistry Chemical Physics* **2018**, 20, 1355-1363
45 Bée, M. Quasielastic neutron scattering. Principles and applications in solid state chemistry, biology and materials science, Adam Hilger, Bristol, UK **1988**.
46 Heinz Maier-Leibnitz Zentrum, SPHERES: Backscattering spectrometer *Journal of large-scale research facilities* **2015**, 1, A30.
47 Wuttke, J.; Budwig, A.; Drochner, M.; Kämmerling, H.; Kayser, F.-J.; Kleines, H.; Ossovyl, V.; Pardo, L- C.; Prager, M.; Richter, D.; Schneider, G. J.; H. Schneider, Staringer, S. SPHERES, Jülich's high-flux neutron backscattering spectrometer at FRM II *Rev. Sci. Instr.* **2012**, 83, 075109.
48 Zorn, R. Multiple scattering correction of neutron scattering elastic scans *Nucl. Instr. Meth. A* **2007**, 572, 874 - 881.
49 Heinz Maier-Leibnitz Zentrum, TOFTOF: Cold neutron time-of-flight spectrometer *Journal of large-scale research facilities* **2015**, 1, A15.
50 Rieutord, F. INX-Program for time-of-flight data reduction, *ILL internal publication* **1990**, 90RI17T.

51 Randl, O. G. SQW - A comprehensive user manual *ILL internal publication* **1996**, 96RA07T.
52 Zorn, R.; Frick, B.; Fetters, L. Quasielastic neutron scattering study of the methyl group dynamics in polyisoprene *Journal of Chemical Physics* **2002**, 116, 845-853.
53 Colmenero, J.; Moreno, A.; Alegria, A. Neutron scattering investigations on methyl group dynamics in polymers *Progress in Polymer Science* **2005**, 30, 1147-1184.
54 Schönhals, A. Schick, C.; Huth, H.; Frick, B.; Mayorova, M.; Zorn, R. Molecular Dynamics in Glass-forming Poly(phenyl methyl siloxane) as Investigated by Broadband Thermal, Dielectric and Neutron Spectroscopy *J. Non-Cryst. Solids* **2007**, **353**, 3853-3861.
55 Konnertz, N.; Böhning, M.; Schönhals, A. Dielectric investigations of nanocomposites based on Matrimid and Polyhedral Oligomeric Phenethyl-Silsesquoxanes *Polymer*, **2016**, 76, 89-101.
56 Prager, M.; Heidemann, A. Rotational Tunneling and Neutron Spectroscopy: A Compilation *Chem. Rev.* **1997**, 97, 2933-2966.
57 Schönhals, A.; Zorn, R. Frick, B. Inelastic Neutron Spectroscopy as a tool to investigate nanoconfined polymer systems *Polymer* **2016**, 195, 393-406.
58 Lau, C. H.; Nguyen, P. T. Hill, M. R.; Thornton, A. W.; Konstas, K.; Doherty, C. M; Mulder, R. J.; Bourgeois, L.; Liu, A. C. J.; Sprouster, D. J.; Sullivan, J. P; Bastow, T. J.; Hill, A. J.; Gin, D. L; Noble, R. D. Ending Aging in Super Glassy Polymer Membranes *Angew. Chem. Int. Ed.* **2014**, 53, 5322 –5326